Appl Phys B (2009) 97: 207–213
DOI 10.1007/s00340-009-3663-0

Applied Physics B
Lasers and Optics

Long distance filamentation of 400 nm femtosecond laser pulses in air

Z. Zhang · X. Lu · T.-T. Xi · W.-X. Liang · Z.-Q. Hao · Y. Zhang · M.-L. Zhou · Z.-H. Wang · J. Zhang

Received: 6 January 2009 / Revised version: 30 May 2009 / Published online: 4 August 2009

Abstract The characteristics of the light filaments formed by $\lambda = 400$ nm blue femtosecond laser pulses are experimentally investigated. Both pre-focused and free propagation conditions are studied. The diameter, length and electron density were measured by using fluorescence signal imaging and longitudinal diffraction method. About 2×10^{17} cm^{-3} electron density in filaments was achieved with beam pre-focusing. In the free propagation case, the multi-filamentation can be observed over 70 m propagation distance, and the energy in the filament core is only about 30 μJ. The effects of energy reservoir on the filament core have been investigated by inserting a diaphragm in a selected single filament path to block the energy of the reservoir. The evolution of filamentation has been studied experimentally as a function of diaphragm size. The energy reservoir can be extended to about 10 mm from the filament core. The results indicate that the up conversion of laser is a possible way to enhance the utilization of laser energy for the generation of long filaments.

PACS 52.38.Hb · 52.35.Mw

Z. Zhang · X. Lu · T.-T. Xi · W.-X. Liang · Z.-Q. Hao · Y. Zhang · M.-L. Zhou · Z.-H. Wang · J. Zhang (✉)
Beijing National Laboratory for Condensed Matter Physics, Institute of Physics, Chinese Academy of Sciences, Beijing 100190, China
e-mail: Jzhang@aphy.iphy.ac.cn

J. Zhang
Department of Physics, Shanghai Jiao Tong University, Shanghai 200240, China

1 Introduction

In recent years there has been great interest in the formation of long light filaments induced by femtosecond (fs) laser pulse in air [1–14]. Many experimental and theoretical studies were performed to investigate the mechanism and the physical properties of laser filaments in air. The propagation of an ultra-intense fs laser pulses in air first undergoes nonlinear Kerr self-focusing effect because of the intensity-dependent refractive index of air. The increased laser intensity due to the self-focusing generates free electrons by the multi-photon ionization (MPI) process, and the electrons contribute negatively to the index of refraction of air. The dynamic balance between the nonlinear Kerr self-focusing and the plasma defocusing due to the MPI and diffraction effects of the laser pulses in air results in the long filamentation of the fs laser pulses.

Up to date, most experimental and theoretical studies on filamentation in air have been performed by using femtosecond pulses with 800 nm wavelength. On this wavelength, the energy of 8 photons is required to ionize the oxygen molecule, and the ionization threshold of laser intensity is about 10^{13} W/cm^2 [15]. MPI occurs much easier if the energy of a single photon becomes higher, so using laser pulses with shorter wavelength is a possible way to enhance the efficiency of the laser energy for generation of plasma filaments in air. Numerous works have also been done to study the filamentation on other wavelengths. The filamentation of UV laser pulses in air has been investigated by using hybrid Ti:sapphire/KrF excimer chain. The filamentation up to 12 m distance with electron density of 10^{16} cm^{-3} was observed [16].

The filamentation of 400 nm femtosecond pulses involving the improvement of beam quality [17] and signal noise ratio of laser pulses [18] was studied last year. A research

group found that the filamentation can be enhanced by using the 400 nm and 800 nm two-colored laser pulses in argon [19]. But to our best knowledge, the detailed characteristics of 400 nm filaments over long distance have not been studied yet. The 400 nm fs laser pulses can be obtained by frequency doubling of 800 nm laser pulses, and it has several characteristics, which are beneficial for the generation of plasma filaments in air. First, the nonlinear refraction index of 400 nm laser in air should be between 4×10^{19} W/cm^{-2} (for $\lambda = 800$ nm [20]) and 8×10^{19} W/cm^{-2} (for $\lambda = 248$ nm [21]), and correspondingly the critical power of self-focusing should be in the range of 0.32–0.64 GW, which is one order less than the critical power of 800 nm laser. Thus, the filamentation occurs much easier on 400 nm wavelength. Second, the ionization ability of the 400 nm photons is much stronger than the infrared waveband. Only 4 photons of 400 nm wavelength are required to ionize the oxygen molecular. Third, the air is still a good transparent medium on 400 nm wavelength. These features of 400 nm laser provide a possibility to generate high quality and long distance filaments. In this paper, we report a detailed experimental investigation on the filamentation characteristics of 400 nm blue fs laser with 6 mJ energy in 170 fs pulse duration. Diagnostics were performed in terms of filaments diameter, length and electron density. The electron density of the filaments was detected by using the longitudinal diffraction method. The filamentation was observed in cases of strong pre-focusing and free propagation. The experimental results showed that to generate the filaments of hundred meters, the 400 nm pulses only require a laser energy of one order less than the 800 nm laser pulses.

2 Electron density measurement

The experimental setup is shown in Fig. 1. A blue fs laser pulse on 400 nm central wavelength with 6 mJ energy is obtained by frequency doubling the 800 nm, 50 fs, 60 mJ infrared pulse, which is delivered from a home-made Ti:sapphire chirped-pulse amplification system. A large aperture (40 mm) KDP crystal of 2 mm thickness is used for frequency doubling. The beam diameter of the blue pulse is about 35 mm. The duration of the blue pulse is estimated to be 170 fs using group-velocity mismatch between the infrared and the blue pulse in KDP crystal [22]. The two wavelength components are separated by the mirror M1, which is fully transparent at 800 nm and high-reflected at 400 nm. The M7, M8 and M9 were coated high-reflected at 800 nm. The blue pulse is used to generate filaments, and the infrared pulse is used as the probe. The pump and the probe pulses are combined by mirror M5, which has the same optical characteristics as M1. The time delay between the pump and the probe pulses can be controlled by delay arms M3, M4 and M6, M7, respectively. The M6 was coated with high-reflected at 800 nm, so only the probe beam is reflected into the CCD. A convex lens is placed on the optical path of 400 nm pulses before mirror M5. The lenses with different focal lengths $f = 1$ m, 2 m and 4 m are used to provide strong initial focusing for the blue pulses, and the plasma filaments can be generated close to the geometric focus of the lenses. The fluorescence of the plasma filaments is imaged by CCD1 with a lens from the side [23]. CCD1 can be moved far from or close to the filaments and the reproduction ratio of the lens can be adjusted in order to retrieve the diameter and the length of the filaments. The diffraction patterns of the probe beam on plasma filaments are recorded by CCD2. The optical path from CCD2 to the filaments is set to be 54 cm, 95 cm and 96 cm for $f = 1$ m, 2 m and 4 m focus lenses respectively. We note that the fluorescence signal from the plasma filaments with pre-focusing by $f = 4$ m lens is too weak and is hardly detected by the normal CCD. Thus, we employ the Electron-Multiplying CCD (EMCCD) to record the fluorescence signal image of this plasma filament.

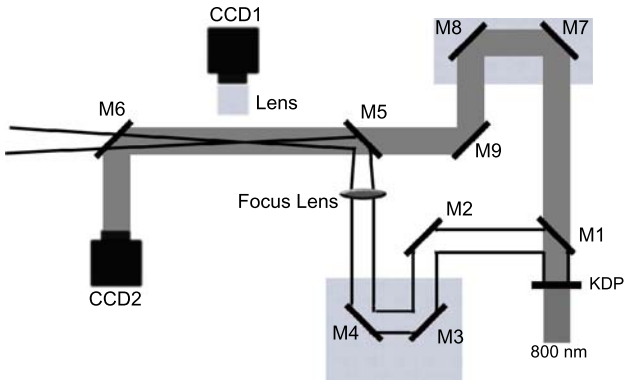

Fig. 1 Experimental setup. The laser beam (400 nm, 6 mJ) is focused in air with thin lenses of focal length $f = 1$ m, 2 m, 4 m, respectively

3 Electron density and analysis

Figure 2(a), (b), (c) show the full image of plasma filaments for pre-focusing lenses $f = 1$ m, 2 m and 4 m, respectively. The curves below the images present the on-axis longitudinal distribution of the fluorescence signal intensity. Figure 2(d), (e), (f) show a close shot of plasma filaments with enhanced transverse resolution for pre-focusing lenses $f = 1$ m, 2 m and 4 m respectively. The curves below present the distribution of fluorescence signal in transverse direction.

From the distribution of fluoresces in transverse and longitudinal direction, as shown in Fig. 2, we can estimate the length and the diameter of the plasma filaments. Both the length and the diameter of the filaments increase with the

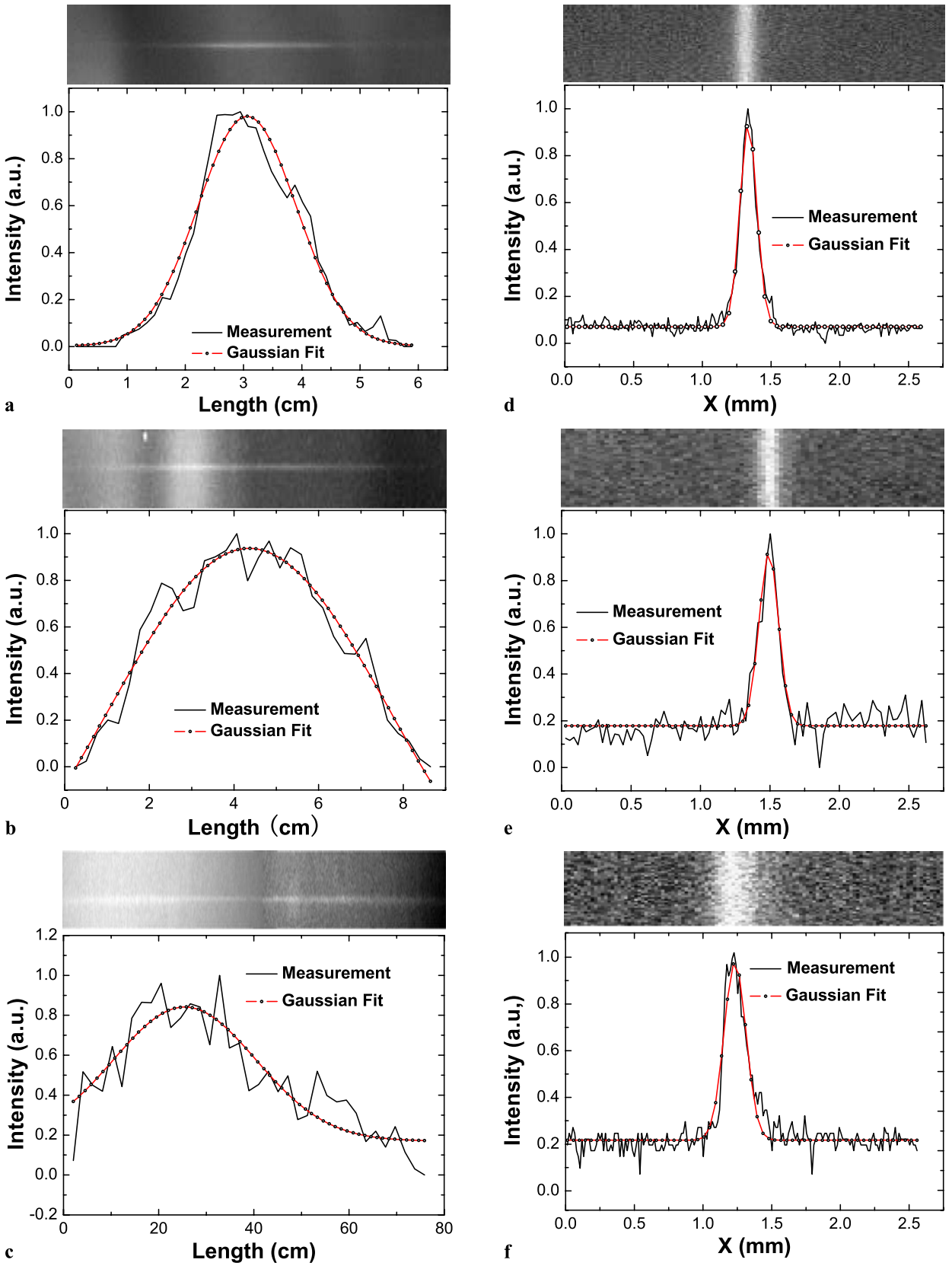

Fig. 2 The fluoresces imaging of filaments. (**a**), (**b**), (**c**) The full images of the filaments for pre-focusing lenses $f = 1, 2, 4$ m, respectively. (**d**), (**e**), (**f**) Close shot of the filaments for pre-focusing lenses $f = 1, 2, 4$ m, respectively

focal length of the pre-focusing lens. The Gaussian approximation of the fluoresces signal distribution is performed for all experimental curves in Fig. 2. The dependencies of the length and diameter(FWHM) of filaments on the focal length of pre-focusing lenses are shown in Fig. 3. Comparably, the diameter and length of the filament, generated by focusing 800 nm laser pulses (6 mJ energy, 50 fs duration) with a $f = 2$ m lens, are 110 μm and 3.5 cm (FWHM), respectively. The size of these 800 nm laser pulses filaments is smaller than that generated by 400 nm laser pulses.

The longitudinal diffraction technique, which is based on the diffraction due to the phase shift induced by the plasma column on the probe pulse propagating collinearly along the filament axis, is employed here to detect the electron density [24]. The delay between the probe and the pump pulses could be adjusted from 0 ps to hundreds of ps. From the diffraction patterns, recorded by CCD2, the phase shift experienced by the probe laser can be reconstructed; thus the electron density can be obtained.

In order to extract the electron density of plasma filaments from the diffraction pattern, we have performed numerical simulations of propagation of the probe pulse. The energy and the diameter of the probe beam are 1.5 mJ and 30 mm respectively. The focus of Kerr self-focusing occurs over 1000 meter away [25]. In this case, the nonlinear effect of the probe pulse can be neglected in the laboratory scale. So it is enough to consider the diffraction and spatial phase modulation due to the electron density in filaments. The propagation of the slowly varying envelope of the probe pulse can be described by the following equation:

$$\frac{\partial E}{\partial z} = i\frac{1}{2k_0}\Delta_\perp E - ik_0\frac{\overline{n_e}}{2n_c}E \tag{1}$$

where z refers to the propagation distance. $k_0 = 2\pi/\lambda_0$ is the central wave number, and $\lambda_0 = 800$ nm is the central wavelength of the probe laser beam. Here the Laplacian operator $\Delta_\perp$ describes the beam transverse diffraction. The profile of the probe beam can be approximately expressed as a super Gaussian function: $E = E_0 \exp(-\frac{r^6}{r_0^6})$, where the diameter r_0 is 3 cm. The electron density produced by the 400 nm laser $\overline{n_e}$ is considered as the average electron density. The parameters L and w are obtained from the side imaging experimental data. Since we assume the average electron density, the diameter and the length data are obtained by the bottom width of the curves in Fig. 2. Due to the cross-phase modulation between the pump and probe pulses; this equation is not valid at zero delay. We substitute different values of $\overline{n_e}$ into (1) and numerically obtain the diffraction pattern of the probe beam on CCD2. The electron density $\overline{n_e}$ can be retrieved, when the simulation result well matches with the pattern obtained from the experiment.

Figure 4(a) shows an example of a diffraction pattern of the probe pulse on the filament produced by using the $f = 1$ m pre-focusing lens, with a delay time 133 ps when the electron density reaches its maximum. Figure 4(b) is a comparison of theoretical and experimental results of diffraction pattern of the probe pulse.

The peak electron density of filaments produced by using different pre-focusing lenses is shown in Table 1. The precision of the electron densities obtained by the fit is 10%

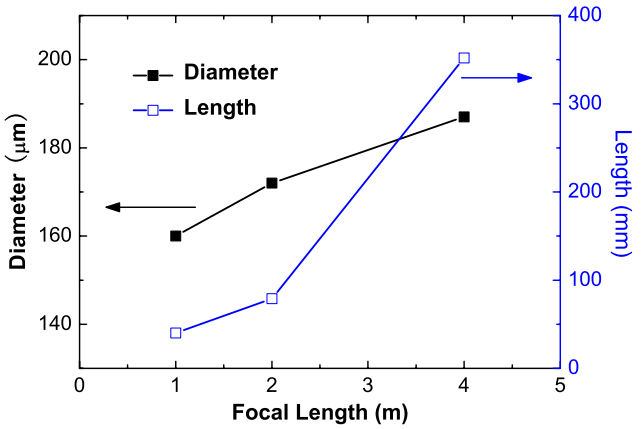

Fig. 3 The filaments diameter and length vary with the pre-focusing lens.

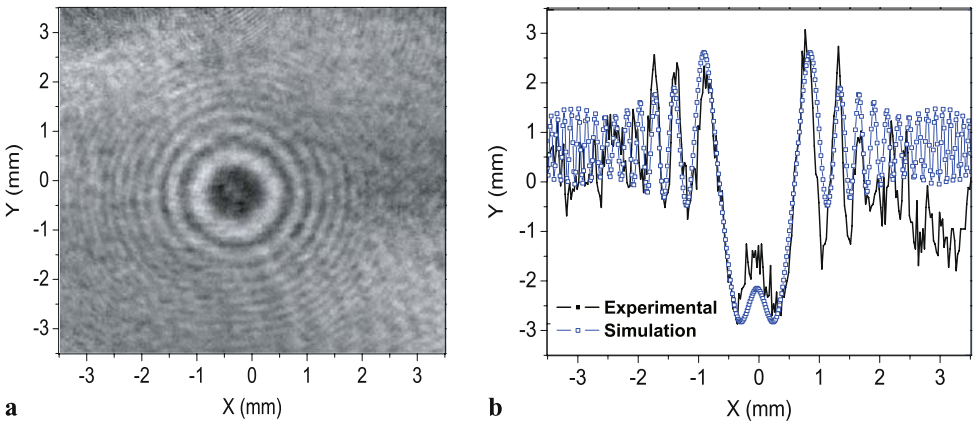

Fig. 4 (**a**) The diffraction pattern of the probe beam for $f = 1$ m lens with delay time of 133 ps. (**b**) Comparison of the simulation result with the experimental measurement of the diffraction pattern

Table 1 The peak electron density of the plasma filaments with pre-focusing lens $f = 1$ m, 2 m and 4 m

Focal length (m)	Electron density (cm^{-3})
1	2×10^{17}
2	8×10^{16}
4	1×10^{16}

for each of the data. The temporal maximum value of electron density is achieved at the delay time 133 ps, and this is mainly caused by the measurement method. The calculation of the electron density is based on the known filament diameter and length, which are taken from the fluorescence image. But the images recorded by the CCD are time integrated. The filamentation, at the beginning, must be multi-filamentation, because the input pulse power is many times higher than the critical power. But due to the diffusion of the electron, the multi-filaments are merged into a more uniform plasma channel, which is recorded by the CCD system. The electron density calculation is based on the diameter and length of this plasma channel, the calculated electron density reaches its maximum value after some delay time.

4 Free propagation

The filamentation of free propagated 400 nm fs laser pulse has also been studied. The 6 mJ pulse was launched freely to a long corridor. The evolution of the beam and the multiple filamentation (MF) was observed. MF was recorded by a CCD camera from a white screen positioned in the beam path at different propagation distance, as shown in Fig. 5. The MF starts at about 24 m distance after the KDP crystal. And the filaments can propagate stably over 70 m without any indication of decline. Meanwhile, the typical filament diameter is about from 0.5 mm to 3 mm in free propagation case, which is one order of magnitude larger than the pre-focused filament. The diameter of the filaments is obtained by measuring the spot size in Fig. 5. Since the filaments are surrounded by a high-intensity photon bath, as well as the conical emission emits at small angles on their side, the diameter of the filaments will be a little overestimated. The measured value can be considered as the upper limit to the diameter. Both the filaments size and positions are stable from shot to shot. The energy in the filament core was measured to be 30 μJ, which is 30 times less than that in the 800 nm free filament [26].

The MF of a free propagated fs laser pulse is observed on one side of the beam, and this situation is mainly caused by the inhomogeneity of the initial laser profile. The bright spots appear at a propagation distance of 24 m on the positions where the local intensity maximum of the initial profile exist. Then these bright spots attract the laser energy around

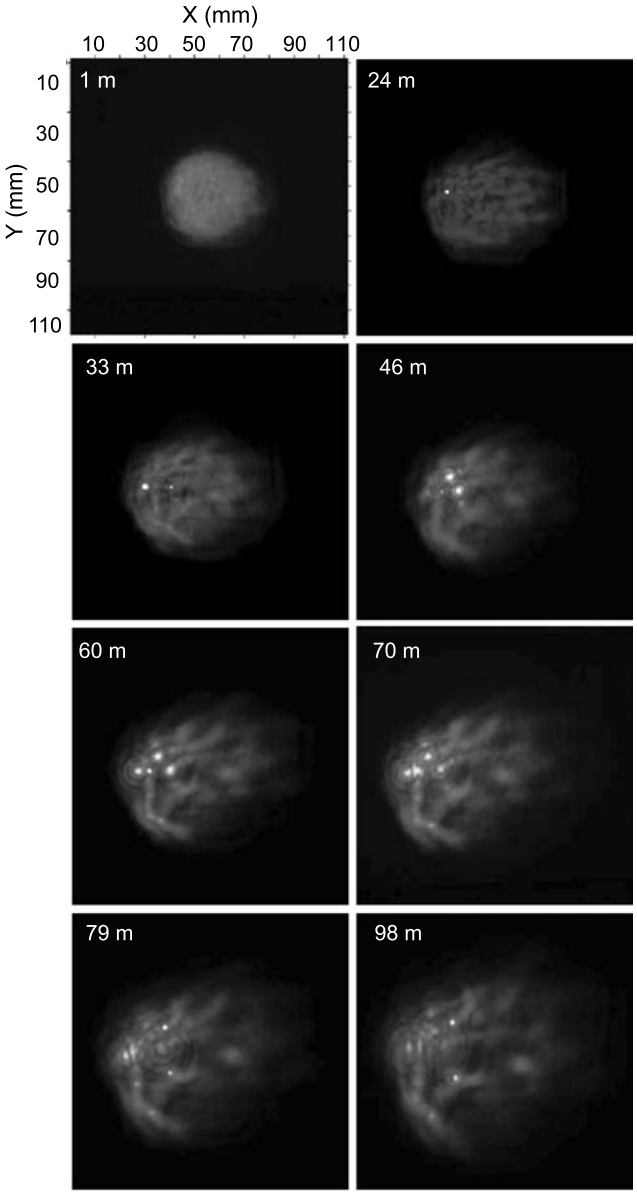

Fig. 5 The filaments patterns on different propagation distances

them and then become primary filaments. These primary filaments lead to a redistribution of the laser energy and produce a new local intensity elevation, from which new filaments can be developed if the power of the local elevation can support self-focusing.

The filaments observed here propagate a distance of 74 meters and the diameter is almost the same. On the other hand, the energy in the filament core is only about tens of micro joules. The filament should be terminated if no energy compensates the energy loss due to the MPI of air and the plasma defocusing. Several experiments have shown that the filament itself contains only about 6–10% of the total pulse energy, while most of the energy is located in the background [27]. The effects of the energy reservoir on the fila-

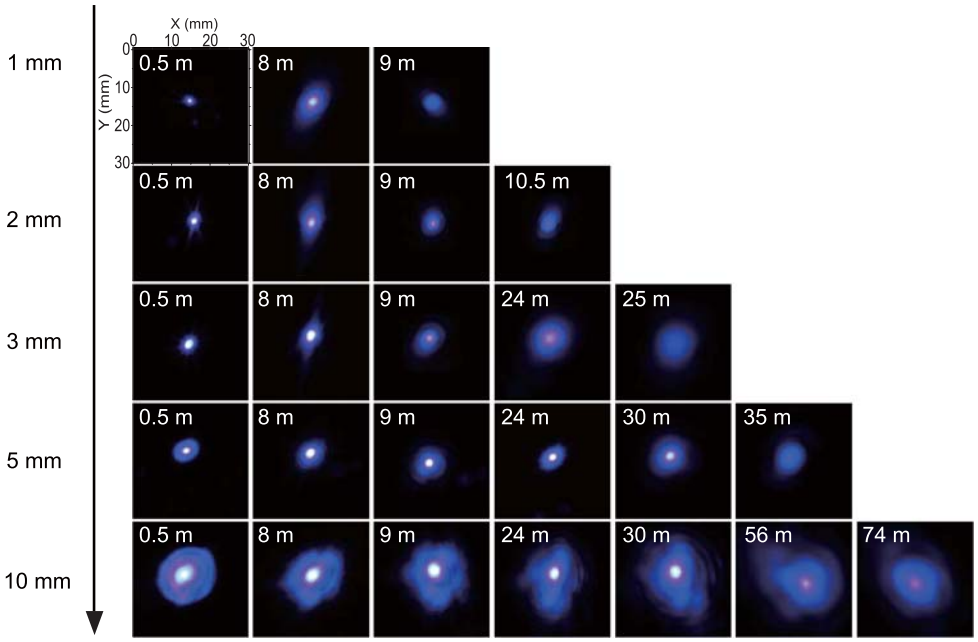

Fig. 6 Intensity profiles of the clipped filament for different diameter diaphragms and propagation distance

ment core have been investigated by inserting a diaphragm in a selected single filament path to block the energy of the reservoir. Here we use the similar method to investigate the properties of energy reservoir of long filaments. The diaphragm is placed at 24 m distance after the KDP crystal with diameter from 1 mm to 10 mm. The filament we choose here has a core diameter of about 0.84 mm. The evolution of the filamentation is shown in Fig. 6 as a function of the diaphragm size. By increasing the size of the diaphragm, the filament can propagate longer distance. With a diameter of 10 mm, the diaphragm admits about 1 mJ energy to pass through, and under this condition, the filament can survive more than 74 m, which reaches the limitation of our laboratory. The same behavior of the energy reservoir was achieved in our previous experiments [28].

5 Conclusions

In conclusion, the filamentation of pre-focused and free fs laser pulse at 400 nm in air have been experimentally and numerically investigated. Our experimental observations clarify the characteristics of the filaments produced by using different focal length lenses and free propagation. In the pre-focusing case, plasma filaments with electron density as high as 2×10^{17} cm^{-3} can be formed. The filaments length increases with the focal length of the pre-focusing lens, but the electron density decreases with the increase of filaments length. In the free propagation case, multiple filaments can be formed and propagate over 74 m. The energy in the core of such large-scale filaments is only 30 μJ, which is 30 times less than that in the filaments of 800 nm wavelength. Our experiments have also demonstrated that the energy reservoir plays a crucial role in the survival and further propagation of filaments. The size and energy of the energy reservoir are important parameters in long-range free propagation of fs laser pulses in air. Most of the energy located in the background serves as an energy reservoir. In our experiment, the energy conversion efficiency of the frequency doubling is only about 10% by using simplest method. But there is great potential to enhance the efficiency of frequency doubling of 800 nm fs laser pulse to about 50% level by using more advanced technology [29–31]. So we expect that up conversion of laser frequency is a possible way to generate high quality filaments in air.

Acknowledgements This work was supported by the National Natural Science Foundation of China under Grant No. 10734130, 10634020, 60621063, National Basic Research Programme of China (No. 2007CB815101).

References

1. A. Braun, G. Korn, X. Liu, D. Du, J. Squire, G. Mourou, Opt. Lett. **20**, 73–75 (1995)
2. B. La Fontaine, F. Vidal, Z. Jiang, C. Chien, D. Comtois, A. Desparois, T. Johnston, J. Kieffer, H. Pépin, H. Mercure, Phys. Plasmas **6**, 1615–1621 (1999)
3. J. Kasparian, R. Sauerbrey, D. Mondelain, S. Niedermeier, J. Yu, J. Wolf, Y.B. André, M. Franco, B. Prade, S. Tzortzakis, A. Mysyrowicz, M. Rodriguez, H. Wille, L. Wöste, Opt. Lett. **25**, 1397–1399 (2000)
4. H. Ladouceur, A. Baronavski, D. Lohrmann, P. Grounds, P. Girardi, Opt. Commun. **189**, 107–111 (2001)
5. H. Yang, J. Zhang, Y. Li, J. Zhang, Y. Li, Z. Chen, H. Teng, Z. Wei, Z. Sheng, Phys. Rev. E **66**, 016406 (2002)

6. H. Yang, J. Zhang, J. Zhang, L. Zhao, Y. Li, H. Teng, Y. Li, Z. Wang, Z. Chen, Z. Wei, J. Ma, W. Yu, Z. Sheng, Phys. Rev. E **67**, 015401 (2003)
7. J. Kasparian, M. Rodriguez, G. Méjean, J. Yu, E. Salmon, H. Wille, R. Bourayou, S. Frey, Y. André, A. Mysyrowicz, R. Sauerbrey, J. Wolf, L. Wöste, Science **301**, 61–64 (2003)
8. G. Méchain, A. Couairon, M. Franco, B. Prade, A. Mysyrowicz, Phys. Rev. Lett. **93**, 035003 (2004)
9. L. Bergé, S. Skupin, F. Lederer, G. Méjean, J. Yu, J. Kasparian, E. Salmon, J. Wolf, M. Rodriguez, L. Wöste, R. Bourayou, R. Sauerbrey, Phys. Rev. Lett. **92**, 225002 (2004)
10. A. Couairon, M. Franco, A. Mysyrowicz, J. Biegert, U. Keller, Opt. Lett. **30**, 2657–2659 (2005)
11. S. Chin, S. Hosseini, W. Liu, Q. Luo, F. Théberge, N. Aközbek, A. Becker, V. Kandidov, O. Kosareva, H. Schroeder, Can. J. Phys. **83**, 863–905 (2005)
12. L. Bergé, S. Skupin, R. Nuter, J. Kasparian, J.-P. Wolf, Rep. Prog. Phys. **70**, 1633–1713 (2007)
13. A. Couairon, A. Mysyrowicz, Phys. Rep. **441**, 47–189 (2007)
14. J. Kasparian, J.-P. Wolf, Opt. Express **16**, 466–493 (2008)
15. G. Méchain, C. D'Amico, Y. André, S. Tzortzakis, M. Franco, B. Prade, A. Mysyrowicz, A. Couairon, E. Salmon, R. Sauerbrey, Opt. Commun. **247**, 171–180 (2005)
16. J. Schwarz, P. Rambo, J. Diels, M. Kolesik, E. Wright, J. Moloney, Opt. Commun. **180**, 383–390 (2000)
17. B. Prade, M. Franco, A. Mysyrowicz, A. Couairon, H. Buersing, B. Eberle, M. Krenz, D. Seiffer, O. Vasseur, Opt. Lett. **31**, 2601–2603 (2006)
18. P. Bejot, C. Bonnet, V. Boutou, J.P. Wolf, Opt. Express **15**, 13295–13309 (2007)
19. P. Béjot, J. Kasparian, J.-P. Wolf, Opt. Express **16**, 14115–14127 (2008)
20. L. Bergé, S. Skupin, G. Méjean, J. Kasparian, J. Yu, S. Frey, E. Salmon, J. Wolf, Phys. Rev. E **71**, 016602 (2005)
21. A. Couairon, L. Bergé, Phys. Rev. Lett. **88**, 135003 (2002)
22. E. Sidick, A. Knoesen, A. Dienes, J. Opt. Soc. Am. B **12**, 1704–1712 (1995)
23. A. Talebpour, S. Petit, S. Chin, Opt. Commun. **171**, 285–290 (1999)
24. J. Liu, Z. Duan, Z. Zeng, X. Xie, Y. Deng, R. Li, Z. Xu, S. Chin, Phys. Rev. E **72**, 026412 (2005)
25. A. Brodeur, C. Chien, F. Ilkov, S. Chin, O. Kosareva, V. Kandidov, Opt. Lett. **22**, 304–306 (1997)
26. Z. Hao, J. Zhang, Z. Zhang, X. Yuan, Z. Zheng, X. Lu, Z. Jin, Z. Wang, J. Zhong, Y. Liu, Phys. Rev. E **74**, 066402 (2006)
27. V. Kandidov, O. Kosareva, A. Koltun, Quantum Electron. **33**, 69–75 (2003)
28. Z. Hao, J. Zhang, X. Lu, T. Xi, Z. Zhang, Z. Wang, J. Opt. Soc. Am. B **26**, 499–502 (2009)
29. T. Kanai, X. Zhou, T. Liu, A. Kosuge, T. Sekikawa, S. Watanabe, Opt. Lett. **29**, 2929–2931 (2004)
30. B. Agate, E. Rafailov, W. Sibbett, S. Saltiel, K. Koynov, M. Tiihonen, S. Wang, F. Laurell, P. Battle, T. Fry, T. Roberts, E. Noonan, IEEE J. Sel. Top. Quantum Electron. **10**, 1268–1276 (2004)
31. A.A. Lagatsky, C.T.A. Brown, W. Sibbett, S.J. Holmgren, C. Canalias, V. Pasiskevicius, F. Laurell, E.U. Rafailov, Opt. Exp. **15**, 1155–1160 (2007)